Applied Thermal Engineering 182 (2021) 116078

Contents lists available at ScienceDirect

Applied Thermal Engineering

journal homepage: www.elsevier.com/locate/apthermeng

The *K* number, a new analogy criterion number to connect pressure drop and heat transfer of sCO_2 in vertical tubes

Haisong Zhang [b], Jinliang Xu [a,b], Xinjie Zhu [b], Jian Xie [a,b,*], Mingjia Li [c], Bingguo Zhu [b]

[a] Key Laboratory of Power Station Energy Transfer Conversion and System, North China Electric Power University, Ministry of Education, Beijing 102206, China
[b] Beijing Key Laboratory of Multiphase Flow and Heat Transfer for Low Grade Energy Utilization, North China Electric Power University, Beijing 102206, China
[c] Key Laboratory of Thermo-Fluid Science and Engineering of Ministry of Education, School of Energy & Power Engineering, Xi'an Jiaotong University, Xi'an, Shanxi 710049, China

ARTICLE INFO

Keywords:
Supercritical carbon dioxide
Friction pressure drop
Heat transfer
Pseudo-boiling

ABSTRACT

Pressure drop and heat transfer are important for design and operation of power plant using supercritical fluid, but they were investigated independently previously. The objective of this paper is to make a connection between pressure drop and heat transfer for supercritical carbon dioxide (sCO_2). Experimental data of pressure drop and heat transfer were obtained in our sCO_2 convective test loop, covering pressures, mass fluxes and heat fluxes in the ranges of 7.5–23 MPa, 500–1500 kg/m^2s and 15–400 kW/m^2, respectively. Different from classical single-phase fluid assumption for supercritical fluid, pseudo-boiling is introduced to deal with flow and heat transfer in supercritical domain, including a wall-attached gas-like layer and a liquid-like fluid in tube core. Supercritical boiling number *SBO* and *K* number are developed to characterize the gas-like layer thickness. Friction factors and heat transfer are found to display the two regimes distribution: a normal heat transfer (NHT) regime with smaller friction factors at smaller *SBO*, and a heat transfer deterioration (HTD) regime accompanying sharply increased pressure drops beyond a critical *SBO*. We conclude an orifice contraction effect due to the strong vapor expansion, explaining the HTD induced rise of pressure drops. We show that *K* can be the similarity criterion number to connect pressure drops and heat transfer. A new correlation of friction factors is developed for sCO_2, which is suitable for NHT and HTD, having mean relative error, mean absolute relative error and root-mean-square relative error of −6.2%, 18.1% and 21.2%, respectively, which are significantly smaller than those predicted by the correlations in the literature.

1. Introduction

The applications of supercritical fluid include the extraction of floral fragrance from flowers, functional food ingredients, pharmaceuticals, cosmetics, powders, and functional materials [1]. Supercritical carbon dioxide (sCO_2) can recover the thermal energy of nuclear reactor into electricity [2]. The sCO_2 Brayton cycles can be driven by various heat sources such as solar energy, waste heat and fossil energy [3–5]. Pressure drop and heat transfer are important for design and operation of power systems, the former determines the compression work for fluid circulation, and the latter determines the heater surface temperatures [6,7].

For convective flow in circular tubes with constant physical properties of single-phase fluid, friction factors are $f = 64/Re$ and $f = 0.3164/Re^{0.25}$ for laminar flow and turbulent flow, respectively, where Re is the Reynolds number [8]. In supercritical pressure, the problem becomes complicated due to the varied physical properties. Pioro et al. [9] reviewed the flow resistance of water and carbon dioxide at supercritical pressure during 1950–1980s. They noted that it was hard to develop satisfactory analytical and numerical methods to calculate friction pressure drop due to the difficulty in dealing with the steep variation of physical properties, especially in turbulent flow at high heat flux. Zhao and Jiang [10] measured friction pressure drops of supercritical R134a cooled in a horizontal tube and compared the results with several available correlations, showing that the Petrov and Popov [11] correlation considering the variations of viscosity and density predicted the experiments reasonably well within ±20%. Jiang et al. [12] measured the friction resistance of supercritical R22 and ethanol in a vertical tube, which was shown to be mainly determined by the density and viscosity

* Corresponding author at: Key Laboratory of Power Station Energy Transfer Conversion and System, North China Electric Power University, Ministry of Education, Beijing 102206, China.
E-mail address: xiejian90@ncepu.edu.cn (J. Xie).

https://doi.org/10.1016/j.applthermaleng.2020.116078
Received 8 May 2020; Received in revised form 26 August 2020; Accepted 14 September 2020
Available online 19 September 2020

Nomenclature

a	coefficients
Bo	boiling number, 1
Ch	non-dimensional number, 1
d	tube diameter, m
e	error
F	force, N
f	friction factor
g	gravitational acceleration, m/s^2
G	mass flux, kg/m^{2}s
i	enthalpy, J/kg
K	non-dimensional number, 1
L	length, m
m	flow rate, kg/s
Nu	Nusselt number
P	pressure, Pa
Pr	Prandtl number, 1
Q	heat created by electrical resistance, W
q	heat flux, W/m^2
Re	Reynolds number, 1
r	radius, m
T	temperature, °C
u	mean velocity
Z	axial flow coordinate

Greek symbols

λ	heat conductivity coefficient, W/m·°C
θ	Angle
ρ	density, kg/m^3
π	Pi
μ	viscosity coefficient, Pa·s
ε	roughness, m
ΔT	temperature overshoot

Subscripts

A	mean relative
ab	absolute
ac	acceleration
ave	average
b	bulk
cr	critical
exp	experiment
f	friction
fg	saturated CO_2turns into saturated vapor
g	gravity
h	hot region
i	inner
in	inlet
iso	isothermal
I’	inertia
l	liquid
M’	momentum
o	outer
out	outlet
pc	pseudo critical
pre	prediction
R	mean absolute relative
S	root-mean-square relative
sat	saturation
v	vapor
w	inner wall
0	saturated liquid at 0 °C

Acronyms

GL	gas-like
HTD	heat transfer deterioration
LL	liquid-like
NHT	normal heat transfer
SBO	supercritical-boiling-number

variations. Fang et al. [13] reviewed the correlations of friction factor at non-isothermal conditions. They stated that none of the existing friction factor correlations was satisfactory in acceptable accuracies, thus they proposed a new one based on 390 experimental data points extracted from available references. The proposed correlation considers tube roughness and reduces the prediction deviation by more than 10% compared with the previous ones. Zhang et al. [14] conducted an experimental investigation of flow resistance of a typical Chinese jet fuel RP-3 flowing through an adiabatic horizontal micro-tube, with reduced pressure ranging from 1 to 2.58, bulk temperature varying from 295 to 789 K, and mass flux up to 1573 kg/m^2 s. They found that friction pressure drops were similar for various pressures at the same mass flux when the reduced temperature was less than 0.95, but the situation is changed when the reduced temperature was larger than 0.95.

Wang et al. [8] measured friction factor of sCO_2 in tubes, with temperature, pressure and Reynolds number ranging from 30 to 150 °C, 3.5–40 MPa, and 200 to 2.0×10^6, respectively. *Re* is thought to reflect the variation of viscosity and density properly, thus a modified correlation of friction factor was proposed. Garimella et al. [15] investigated the cooling of refrigerant blends R404A and R410A in horizontal tubes, with the reduced pressure ranging from 1.0 to 1.2, temperature from 30 to 110 °C, and mass flux from 200 to 800 kg/m^2 s. They modified the Churchill friction factor model based on their experimental data and found that the modified one predicted 74% of the entire data within ±25%. Wang et al. [16] measured pressure drops and friction factors of supercritical water in an annular channel. The gap and the channel length were 4 mm and 1400 mm, respectively. They showed the significant increase of frictional pressure drops when the bulk enthalpy exceeds the pseudo-critical enthalpy. Zang et al. [17] investigated flow resistance of supercritical water in a 2 × 2 rod bundles. The operation pressures focus on 23, 24 and 25 MPa, while the mass flux ranges from 600 to 1400 kg/m^2 s and the heat flux is up to 943 kW/m^2. Friction coefficients are observed to have the “V” shape versus *Re*. They pointed out that the physical property differences between wall and bulk fluid should be considered. The heat flux and mass flux would affect the friction coefficient through changing the material correction factor. Fang et al. [18] reviewed the correlations of friction factor of turbulent pipe flow under supercritical pressure. Two databases including 1279 experimental data points were cited from 12 references (820 data points for adiabatic conditions and 459 data points for non-isothermal conditions). Six adiabatic and 13 non-isothermal correlations are evaluated. A new model for adiabatic supercritical fluids is developed. Because friction pressure drop is influenced by heat flux, mass flux, flow orientation and tube diameters, more data should be achieved for sCO_2 [19]. Based on the single-phase fluid assumption, the varied physical properties and buoyancy/acceleration effect are used to explain the distinct thermal-hydraulics in supercritical pressure [20,21]. Friction factor at non-isothermal condition has been considered by the corrections of physical properties such as density, viscosity and Prandtl number [22–24].

Supercritical heat transfer (SHT) is another important topic. When crossing pseudo-critical point, heat transfer is either enhanced or deteriorated [20,25,26]. To develop power plants driven by nuclear energy or fossil energy, fruitful water data of SHT have been obtained since 1950s [27]. However, experimental data are insufficient for sCO_2 power plants. Experiment data were obtained near the critical pressure ~8 MPa [28], noting that a practical S-CO_2 cycle operates in pressures in the range of 20–30 MPa [29]. Similar to friction factors, SHT is treated with the single-phase fluid assumption [30,31]. The varied physical properties and buoyancy/acceleration effects are believed to cause abnormal heat transfer for more than half century [32]. Recent works show that the buoyancy and acceleration effects are not success to calculate heat transfer coefficients, several review papers comment on this issue [20,31,32].

The above literature survey concludes that: (i) The available friction factor correlations are based on the single-phase fluid assumption with the corrections of physical properties. These correlations are different one by one, and the prediction accuracies should be further improved [9,13]. (ii) It is sure that both normal heat transfer and heat transfer deterioration can occur in supercritical domain [20,25]. However, there are no experimental data and theoretical work on flow resistance when heat transfer deterioration occurs. (iii) Flow resistance and heat transfer are investigated separately. The link between flow resistance and heat transfer has not been established.

The objective of this paper is to make a connection between flow resistance and heat transfer. Both flow resistance and heat transfer are studied experimentally and theoretically. The original contribution of this paper is summarized as follows. First, different from the classical treatment of flow and heat transfer for supercritical fluids, the single-phase fluid assumption is abandoned. Instead, pseudo-boiling is introduced. SHT under heating condition includes a two-fluids structure: a gas-like fluid near wall, and a liquid-like fluid in tube core. The inhomogeneous structure of supercritical fluid has received attention by physicists [33–36], but has not received attention in the community of engineering. Second, two important parameters of supercritical boiling number *SBO* and *K* are shown to be related to the gas-like layer thickness, which are key to dominate flow and heat transfer.

Both flow resistance and heat transfer are found to display the two regimes distribution. The normal heat transfer (NHT) regime does not have wall temperature overshoot accompanying smaller pressure drops. Beyond a critical *SBO*, NHT is suddenly switched to heat transfer deterioration (HTD), with significantly increased friction factors. The *K* number is identified as the similarity criterion number to connect friction pressure drops and heat transfer. A new correlation of friction factors is presented, which is suitable for both NHT and HTD. The increased pressure drop for HTD is explained by the orifice contraction effect occurring at the tube cross-section having the wall temperature peak. The finding of this paper is important, because based on our present work, we understand that heat transfer deterioration not only causes the abrupt rise of wall temperatures, but also yields the sharp rise of pressure drops. The former threatens the safety of heater surface, and the latter increases the load and compression power for compressors, hence heat transfer deterioration should be avoided for design and operation of power plants.

2. Experimental apparatus and data reduction

2.1. Experimental system

The available experiments on sCO_2 heat transfer were reported near the critical pressure ~8 MPa [28], which is sufficiently lower than the operation pressure of sCO_2 cycles. To develop sCO_2 power cycles driven by nuclear energy, solar energy and fossil energy, a sCO_2 flow and heat transfer test loop has been built in North China Electric Power University (China), with the maximum pressures, temperatures and heat fluxes up

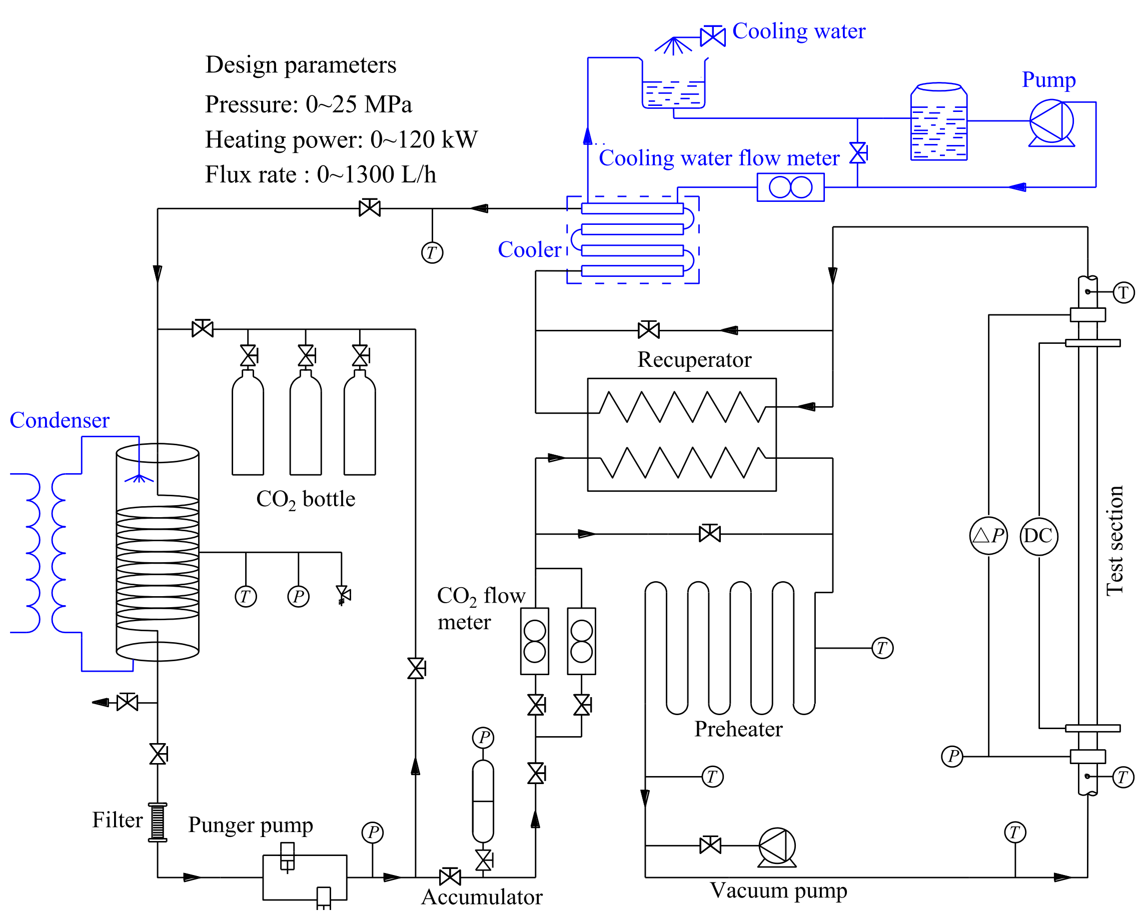

Fig. 1. Experimental setup.

to 25 MPa, 500 °C and 400 kW/m^2, respectively. Fig. 1 shows the experiment setup, including a forced convective loop, a coolant circulation loop and a measurement system. The CO_2 convective loop was vacuumed to remove non-condensable gas and charged with the 99.99% purity CO_2 before formal experiment. The CO_2 liquid is driven by a plunger pump, then it is heated to a required temperature in a recuperator heat exchanger and a preheater before entering the test section. The preheater and test section are heated by an electric power supply system with a maximum capacity of 54 kW. At the test section outlet, the CO_2 vapor was consecutively cooled by the recuperator heat exchanger, a cooler and a condenser. A cooling water loop dissipates heat from the cooler, and an ethylene glycol solution dissipates heat from the condenser.

The measurement system collects the experimental data. The flow rate of CO_2 is measured by one of the two flow meters (DMF-1-3) with an uncertainty of 0.2%. At the test section inlet, the CO_2 pressure is stabilized by an accumulator and measured by a pressure transducer (Rosemount 1151) with an uncertainty of 0.2%. The pressure drop of CO_2 across a 2.4 m length test section is measured by a pressure drop transducer (Rosemount 3051) with an uncertainty of 0.1%. The heating power applied to the test section is controlled by a DC voltage provided by the power supply system. Temperatures are measured by K-type thermocouples with an uncertainty of 0.5 °C.

2.2. *The test tube*

The present paper focuses on pressure drops of sCO_2 in vertical tubes with upward flow direction. Additional experimental data were achieved for the inner diameters of 8.0 mm and 12.0 mm. Thus, three groups of data with d_i = 8.0, 10.0 and 12.0 mm were used in this paper.

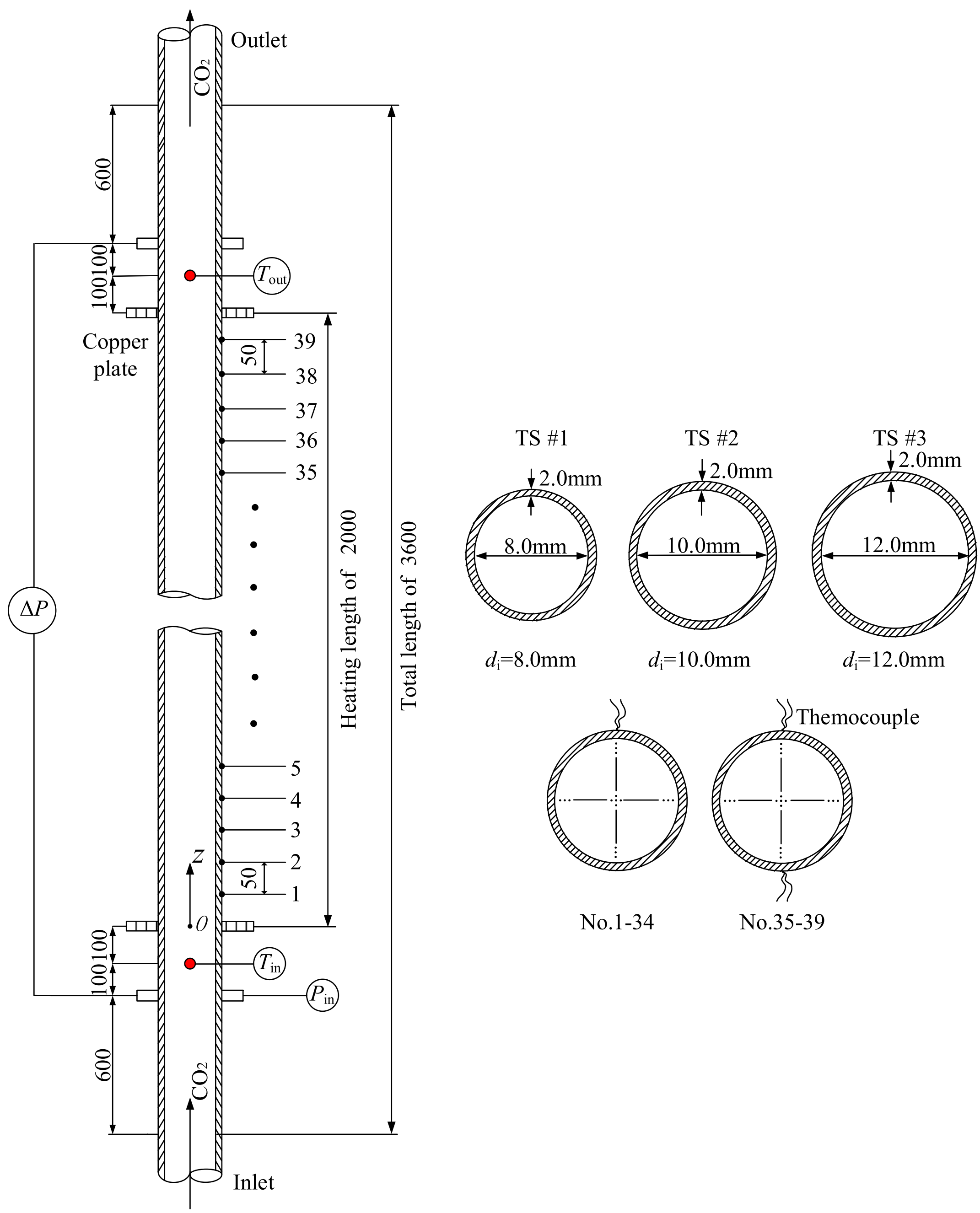

Fig. 2. The three test tubes used in the present study.

Fig. 2 shows the test tube made of 1Cr18Ni9Ti. All the sizes in length direction are identical for the three test tubes. The total length of test tube is 3600 mm including two stabilization sections, one is ahead of the major test section and the other is beyond the major test section. The major test section has a 2400 mm length across a differential pressure drop transducer. The heating section is 2000 mm in length, and the wall thickness is 2.0 mm. The test tube is heated by the DC (direct-current) power via two electrodes across a heating length of 2000 mm. Thermocouple wires are welded on the outer wall by a capacitance impact welding machine. Thus, thermal resistance between thermocouple and tube wall does not exist. These thermocouples are arranged on 39 cross-sections along flow direction. The axial distance between two neighboring cross-sections is 50 mm. Cross-sections 1–34 have a single thermocouple, but cross-sections 35–39 have two thermocouples. Due to the geometry symmetry, the two readings of thermocouples on a specific cross-section are almost identical. The test tube is wrapped by a thermal insulation material with ultra-low thermal conductivity. After the test loop is ready, repeatable experiments were performed (see Fig. 3). It is shown that the same running parameters yield almost the same results, for both normal heat transfer (NHT) and heat transfer deterioration (HTD). These results were obtained in different days, in which $T_{w,o}$ means the outer wall temperature.

2.3. Data reduction

The total pressure drop in a channel is expressed as

$$\Delta P = \Delta P_f + \Delta P_g + \Delta P_{ac} \tag{1}$$

where ΔP is the measured pressure drop, the subscripts *f*, *g* and *ac* mean the pressure drops of friction, gravity and acceleration component, respectively. The acceleration pressure drop is

$$\Delta P_{ac} = \rho_{out}u_{out}^2 - \rho_{in}u_{in}^2 = G^2\left(\frac{1}{\rho_{out}} - \frac{1}{\rho_{in}}\right) \tag{2}$$

where ρ is the density, u is the mean velocity, G is the mass flux, the subscripts *out* and *in* represent the inlet condition and outlet condition, respectively.

The gravity pressure drop is

$$\Delta P_g = \int_{-0.2}^{L-0.2} \rho g sin\theta \mathrm{d}z \tag{3}$$

where z is the axial flow coordinate with the original point starting from the bottom electrode, L is the length across the pressure drop transducer (here $L = 2.4$ m in Fig. 2), g is the gravity acceleration, θ is the inclination angle with respect to the horizontal plane.

For vertical tube with upward flow direction, θ is 90°. Then,ΔP_g is

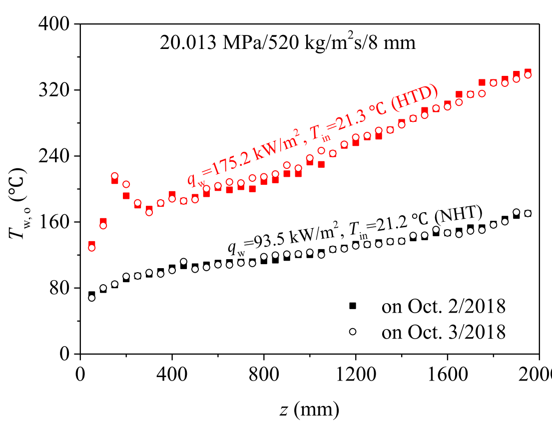

Fig. 3. Repeatable experiment for normal heat transfer (NHT) and heat transfer deterioration (HTD).

reduced to

$$\Delta P_g = \left(\frac{T_{b,in}\rho_{in} - T_{b,out}\rho_{out}}{T_{b,in} + T_{b,out}}\right)gL \tag{4}$$

where $T_{b,in}$ and $T_{b,out}$ are the bulk fluid temperature at the inlet condition and outlet condition, respectively.

Thus, the friction pressure drop is

$$\Delta P_f = \Delta P - \Delta P_g - \Delta P_{ac} = f\cdot\frac{L}{d_i}\cdot\frac{G^2}{2\rho_{ave}} \tag{5}$$

where f is the friction factor, ρ_{ave} is the density defined at the average temperature of $0.5(T_{b,in} + T_{b,out})$.

The mass flux is

$$G = m/\left(\frac{1}{4}\pi d_i^2\right) \tag{6}$$

The effective heating power applied to the test tube Q and the inner wall heat flux q_w are

$$Q = m\left(i_{b,out} - i_{b,in}\right),\ \ q_w = Q/(\pi d_i L_h) \tag{7}$$

where m is the mass flow rate, $i_{b,in}$ and $i_{b,out}$ are the bulk fluid enthalpies at inlet condition and outlet condition, L_h is the heating length ($L_h = 2.0$ m in Fig. 2). The axial length dependent fluid enthalpy i_b is

$$i_b(z) = i_{b,in} + \frac{\pi q_w d_i z}{m} \tag{8}$$

We note that the heating power is uniformly applied to the test tube through the resistance heating of the tube material. The one-dimensional heat conduction equation is used to determine the inner wall temperature $T_{w,i}$ based on the measured outer wall temperature $T_{w,o}$:

$$\frac{1}{r}\frac{d}{dr}\left(r\lambda\frac{dT}{dr}\right) + q = 0 \tag{9}$$

where λ is the thermal conductivity of the tube, r is the radial coordinate. Eq. (9) satisfies the following boundary condition:

$$\left.\frac{dT}{dr}\right|_{r=r_o} = 0,\ \ T|_{r=r_o} = T_{w,o} \tag{10}$$

where r_o is the outer tube radius, q is the heat generation rate per unit volume due to the resistance heating:

$$q = \frac{Q}{\pi\left(r_o^2 - r_i^2\right)L_h} \tag{11}$$

Eq. (9) subjecting to Eqs. (10) and (11) yields $T_{w,i}$ as

$$T_{w,i} = T_{w,o} - \frac{q_w r_i}{2\lambda}\left(\frac{a^2 - 2lna - 1}{1 - a^2}\right) \tag{12}$$

where a is the ratio of inner tube radius to outer tube radius: $a = r_i/r_o$. Table 1 summarizes the ranges and uncertainties of various parameters.

Table 1
Uncertainties and ranges of various parameters.

Value	Range	Uncertainty
Pressure P	7.5–23 MPa	1%
Differential pressure $\triangle P$	0–20 kPa or 0–50 kPa	2.06%
Inlet fluid temperature $T_{b,in}$	10–120 °C	0.5 °C
Out fluid temperature $T_{b,out}$	25–200 °C	0.5 °C
Outer wall temperature $T_{w,o}$	30–450 °C	0.5 °C
Mass flow flux G	500–1500 kg/m^{2}s	2.05%
Heat flux q_w	15–400 kW/m^2	5.05%
Friction coefficient f	0.005–0.06	3.0%

3. Pseudo-boiling and non-dimensional parameters

Pseudo-boiling was mentioned in 1960s [37,38], but it has been seldom used to treat SHT theoretically or numerically. The physical properties such as heat capacity, thermal expansion coefficient and isothermal compressibility reach maxima at the pseudo-critical point in supercritical pressure. Because these maxima do not belong to the first-order liquid-gas phase transition, they are called critical anomalies [39]. By inelastic X-ray scattering and molecular dynamics, Simeoni et al. [33] showed that the Widom line divides the fluid into a liquid-like LL region and a gas-like GL region. Similar conclusion was drawn by McMillan and Stanley [34]. Ha et al. [35] analyzed the density fluctuations and demonstrated that when the fluid temperatures are varied over a wide range at a supercritical pressure, three regimes including LL, liquid-gas coexistence, and GL occur in the *P-T* phase domain, very similar to those in subcritical pressure. By neutron imaging technique, Maxim et al. [40] succeeded to monitor density fluctuations of supercritical water while the system evolves rapidly from LL to GL during isobaric heating. They showed that the Widom line can be identified experimentally and they agree with the pseudo-boiling theory.

We start from the analogy between subcritical boiling and SHT. For the former, when T_b is lower than T_{sat}, a high heat flux q_w gives rise to bubble nucleation and growth on tube wall (see Fig. 4a). Further increase of q_w causes the coalescence of bubbles to form a vapor blanket (see Fig. 4b). Because the vapor layer has low thermal conductivity, Fig. 4b corresponds to poorer heat transfer compared to Fig. 4a. The transition from Fig. 4a to b is related to if bubbles can be successfully departed from the wall, for which two forces are competed with each other (see Fig. 4c). One is the inertia force having the tendency to detach the bubble from the wall ($F_{I'}$), and the other is the evaporation momentum force having the tendency to adhere the bubble on the wall ($F_{M'}$). The *K* number is [41]:

$$K = \frac{\text{evaporation momentum force}}{\text{inertia force}} = \left(\frac{q_w}{G \cdot i_{fg}}\right)^2 \frac{\rho_l}{\rho_v} = Bo^2 \frac{\rho_l}{\rho_v} \tag{13}$$

where i_{fg} is the latent heat of evaporation, ρ_l and ρ_v are the densities of liquid and vapor, respectively, $Bo = q_w/(Gi_{fg})$ is the boiling number, reflecting the comprehensive effect of heat flux, mass flux and pressure. A smaller *K* represents easier departure of bubbles from the wall, but a larger *K* means the difficulty in departing bubbles (see Eq. (13)). *Bo* and *K* have been shown to be useful for subcritical boiling [41].

Recently, pseudo-boiling is introduced by the present authors [42–44]. For a supercritical fluid heated by a channel wall, the flow structure consists of a gas-like GL layer near wall and a liquid-like LL fluid in tube core when $T_w > T_{pc} > T_b$ (see Fig. 4d-e), where T_{pc} and T_b are the pseudo-critical temperature and bulk temperature at a tube cross-section. The two regions of fluids are interfaced at $T = T_{pc}$, also called the Widom line. By the analogy to subcritical boiling, supercritical boiling number *SBO* is defined as

$$SBO = \frac{q_w}{G \cdot i_{pc}} \tag{14}$$

where i_{pc} is the enthalpy at pseudo-critical temperature. *SBO* comprehensively reflects the effects of heat flux, mass flux and pressure. We show that when the tube diameter is in the range of 2.0–10.0 mm, NHT can be suddenly switched to HTD when crossing a critical *SBO*, which is 5.126×10^{-4} for sCO_2 for upward flow [42]. This conclusion is also valid for other working fluids, but different working fluid has different critical *SBO* [43]. The *K* number in supercritical pressure is defined as

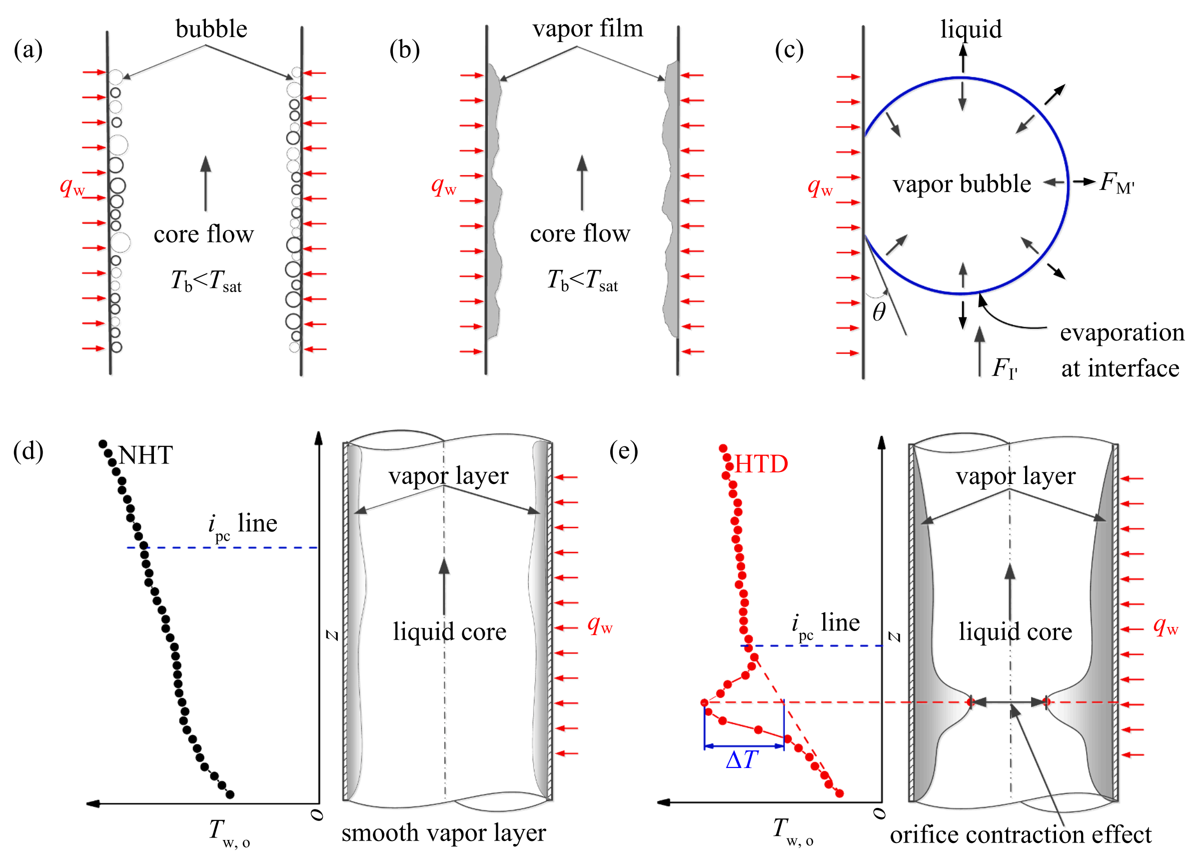

Fig. 4. The flow pictures for subcooled boiling at subcritical pressure and supercritical heat transfer (a: isolated bubbles on tube wall at subcritical pressure; b: vapor blanket formation on tube wall at subcritical pressure; c: two forces are competed on bubble at subcritical pressure; d: normal heat transfer for supercritical heat transfer with $P = 20.013$ MPa, $G = 520$ kg/m^{2}s, $d_i = 8$ mm and $q_w = 96.8$ kW/m^2; e: heat transfer deterioration for supercritical heat transfer with $P = 8.021$ MPa, $G = 1000$ kg/m^{2}s, $d_i = 8$ mm and $q_w = 265.5$ kW/m^2).

[44]

$$K = \left(\frac{q_w}{G \cdot i_w}\right)^2 \frac{\rho_{LL}}{\rho_{GL}} \tag{15}$$

where i_w is the enthalpy at the inner wall temperature $T_{w,i}$, ρ_{LL} and ρ_{GL} are the densities for liquid-like fluid and gas-like fluid, respectively. To reflect the effect of $T_{w,i}$, Eq. (15) is reduced to [44]

$$K = \left(\frac{q_w}{G \cdot i_w}\right)^2 \frac{\rho_b}{\rho_w} \tag{16}$$

where ρ_b and ρ_w are the densities at bulk fluid temperature and inner wall temperature. K represents the competition between evaporation momentum force and inertia force. Using 5560 experimental data points, a general correlation is developed as $Nu = 0.0012Re_b^{0.9484}Pr_{b,ave}^{0.718}K^{-0.0313}$ to

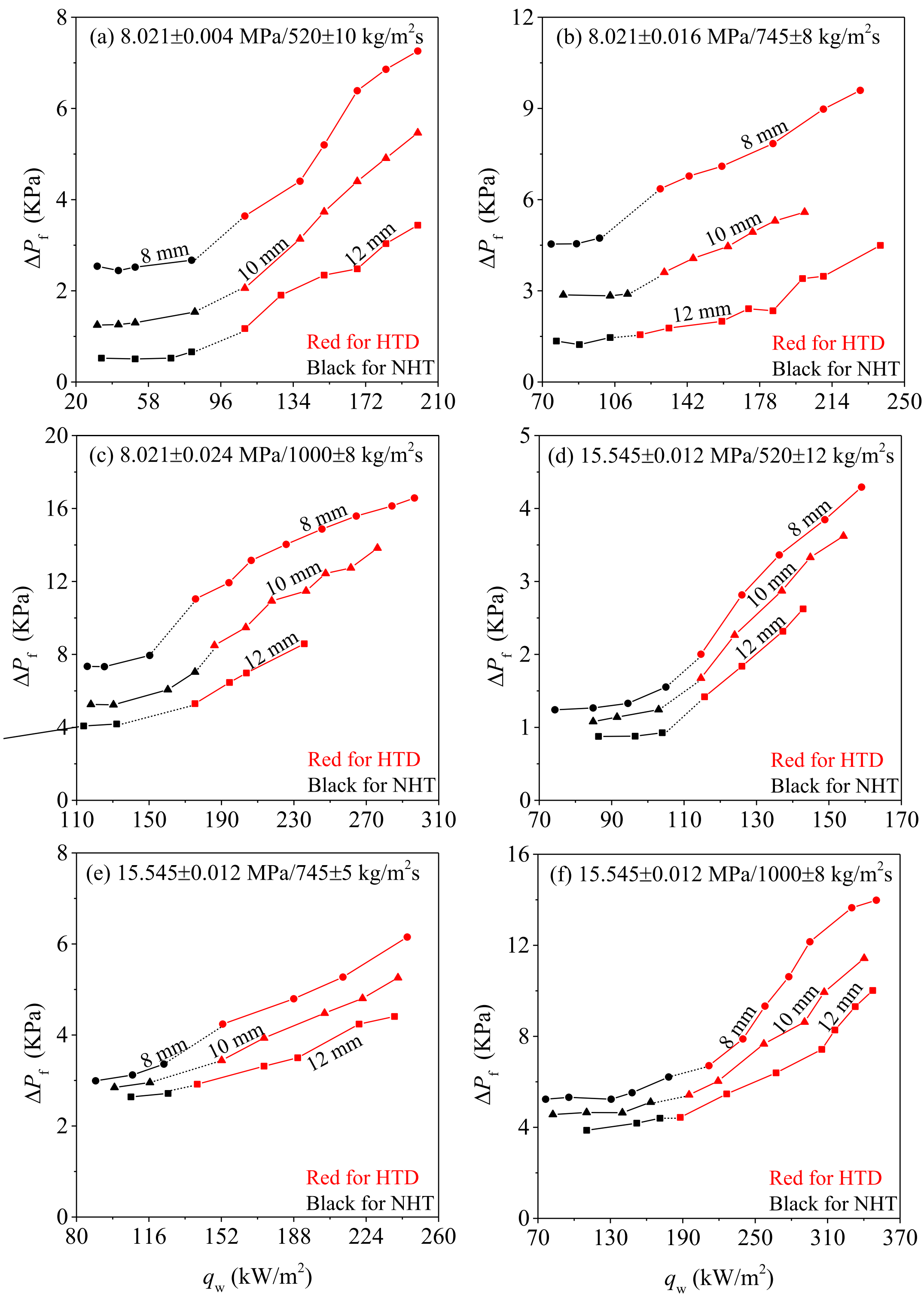

Fig. 5. Effect of heat fluxes on frictional pressure drops.

predict heat transfer coefficients, where Re_b and $Pr_{b,ave}$ are the Reynolds number and average Prandtl number defined at bulk fluid temperature on each tube cross section [44]. The prediction accuracy is better than the widely cited correlations in the literature.

The present paper focuses on the connection between pressure drop and heat transfer in supercritical domain. A NHT case behaves a gentle rise of wall temperatures along flow direction (see Fig. 4d), but a HTD case results in a sharp wall temperature peak with $i_b < i_{pc}$ (see Fig. 4e). Heat transfer is recovered beyond the temperature overshoot. For HTD, a wall temperature overshoot corresponds to a large K and a locally expanded vapor-like layer thickness (see Fig. 4e). This is equivalent to artificially arrange a solid orifice on the cross-section corresponding to the wall temperature peak, introducing an additional pressure drop due to local fluid restriction, which is called the orifice contraction effect in this paper. Latter we will show that the link between pressure drop and heat transfer does exist for sCO_2 heat transfer in vertical tubes with upward flow direction.

The Reynolds number Re is

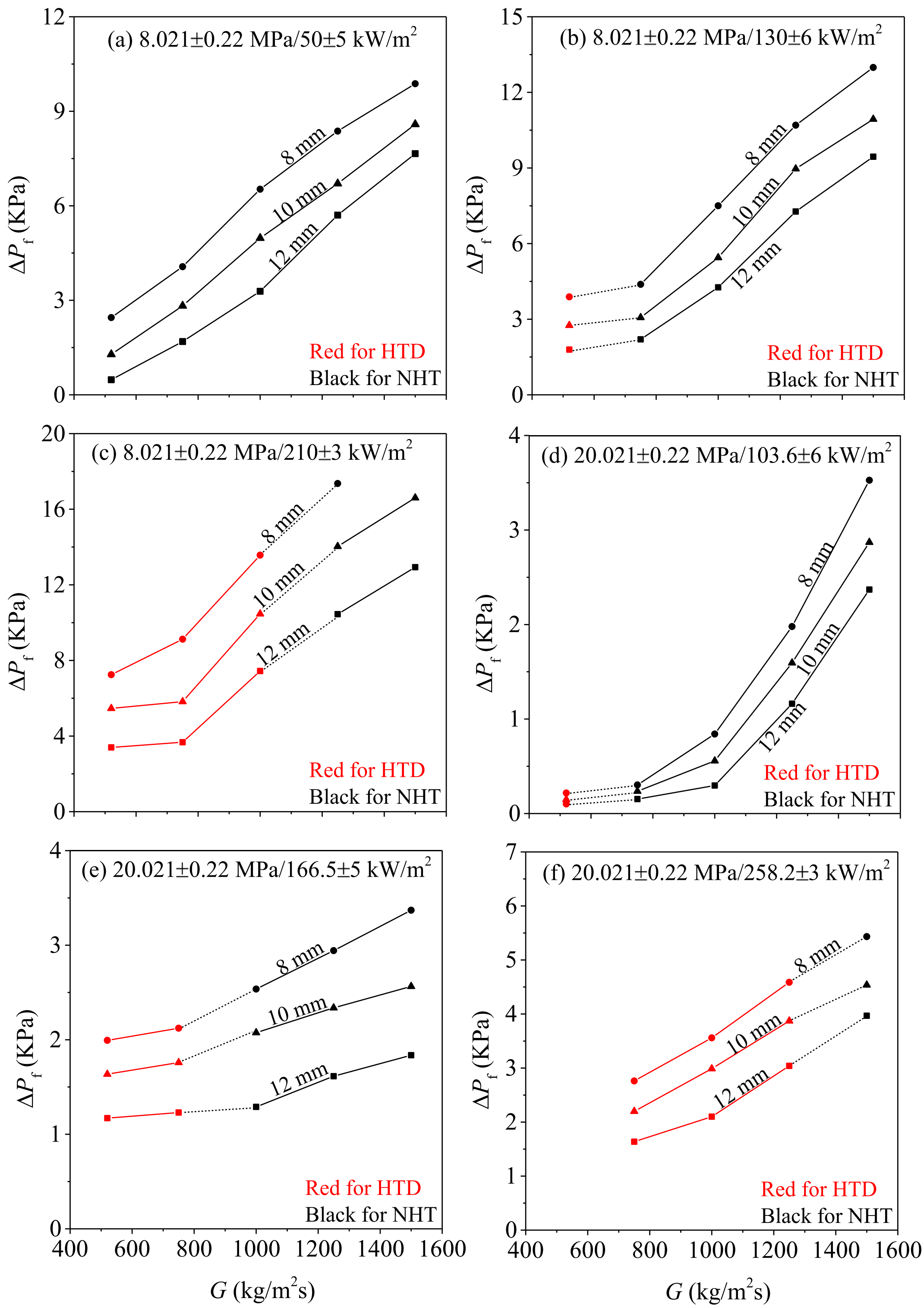

Fig. 6. Effect of mass fluxes on the frictional pressure drops.

$$Re = \frac{G \cdot d_i}{\mu_{b,\,ave}} \tag{17}$$

where $\mu_{b,ave}$ is the viscosity at the average bulk fluid temperature between inlet and outlet, $T_{b,ave} = 0.5(T_{b,in} + T_{b,out})$. Here, we present a friction coefficient correlation incorporating both NHT and HTD runs. For NHT, K in Eq. (16) is defined at $T_{b,ave}$. The wall condition w corresponds to the cross-section corresponding to $T_{b,ave}$. For HTD, the parameters in Eq. (16) are defined at the tube cross-section corresponding to wall temperature peak to reflect the orifice contraction effect.

4. Result and discussion

4.1. Effects of various parameters on frictional pressure drop

In this paper, P, G and q_w are varied in the ranges of 7.5–23 MPa, 500–1500 kg/m^2 s and 15–400 kW/m^2, respectively. The tube diameters are $d_i = 8.0$, 10.0 and 12.0 mm. Effect of various parameters on friction pressure drops is explored (see Figs. 5 and 6), in which data points with black and red colors represent normal heat transfer (NHT) and heat transfer deterioration (HTD), respectively. Smaller tube diameter gives rise to larger friction pressure drops when other parameters are identical, which is true for all the tests in this paper. This phenomenon is explained by the fact that ΔP_f is inversely proportion to d_i (see Eq. (5)).

When other parameters are almost identical, heat flux obviously influences friction pressure drops (see Fig. 5). ΔP_f displays the two regimes distribution, which is smaller at smaller q_w (black data points), but increases sharply when q_w attains a specific value (read data points). The slopes of $\Delta P_f \sim q_w$ are weak for NHT, but become significant for HTD, demonstrating that pressure drops are strongly dependent on if HTD occurs.

Fig. 6 presents the effect of G on ΔP_f. ΔP_f increases with increase of G, which can be explained by Eq. (5) to indicate that ΔP_f is a function of f, L, d_i, G and ρ_{ave}. Especially, the scale law of $\Delta P_f \sim G^2$ explains the quick rise of ΔP_f by increasing G. Previously, friction factors f are correlated with the correction terms of physical properties defined at bulk fluid temperature relative to the values defined at wall temperature [22–24]. Some f correlations introduce the correction term of q_w/G [11]. Because q_w/G is not a non-dimensional parameter, it does not reflect physical mechanism regarding SHT. The observed trends of ΔP_f can be easily explained by pseudo-boiling. Usually, two-phase flow has larger ΔP_f than single-phase flow. The increase trend becomes significant with increase of vapor mass qualities [45]. The introduction of bubbles on tube wall is equivalent to increase tube wall roughness to raise shear stress on the wall. The interaction between gas and liquid phases increases energy dissipation to increase the pumping power of two-phase system. In supercritical pressure, pseudo-boiling assumes a gas-like GL layer on tube wall and a liquid-like LL fluid in tube core. This flow picture is equivalent to introduce an additional wall roughness to increase friction pressure drops.

We note that the six subfigures in Fig. 5 contain the experiment data in two pressure levels of ~8 MPa and ~15 MPa. Alternatively, Fig. 6 involves two pressure levels of ~8 MPa and ~20 MPa. When mass fluxes are similar (see Fig. 5b and e at $G = 745$ kg/m^2 s, and Fig. 5c and f at $G = 1000$ kg/m^2 s), higher pressures lowers friction pressure drops, indicating the weakened pseudo-boiling effect with increase of pressures. Our recent papers show that heat transfer coefficients are increased with increase of pressures [44]. The present paper identifies the reduced friction pressure drops when pressures are increased.

4.2. The two regimes of heat transfer and friction pressure drops

Figs. 7 and 8 present heat transfer and friction pressure drops, respectively. One notes that each run has a SBO defined by Eq. (14). Effect of SBO on heat transfer is examined first, for which wall temperature overshoot (ΔT) is defined in Fig. 7c. Using the experiment data

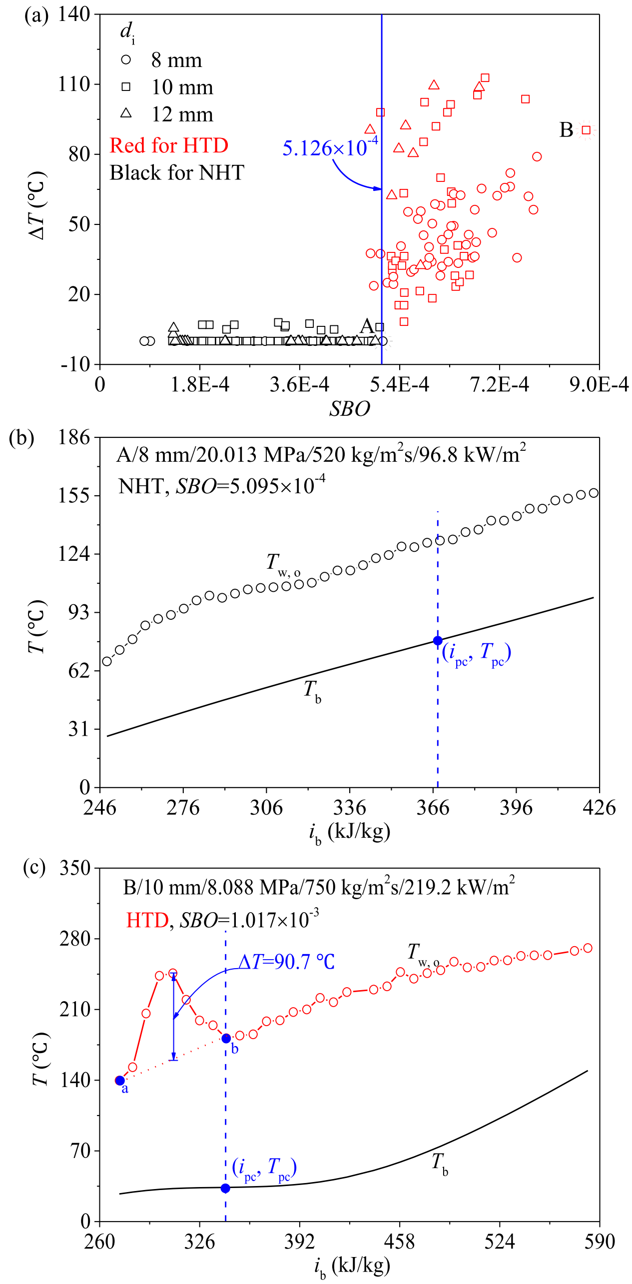

Fig. 7. The critical SBO dominates the transition from normal heat transfer to heat transfer deterioration (a: the two regions of heat transfer interfaced by the critical SBO; b: NHT case; c: HTD case).

with $d_i = 2$–10 mm, we conclude a critical $SBO_{cr} = 5.126 \times 10^{-4}$ as the transition boundary from NHT to HTD [42]. Here, additional data are provided with $d_i = 8.0$ mm and 12.0 mm. Data points with additional tube diameters do not change the critical SBO for the transition boundary. In Fig. 7a, point A is marked for NHT but point B is marked for HTD. The wall temperature curve indicates no temperature overshoot for NHT (see Fig. 7b), in which T_b and i_b are bulk fluid temperature and enthalpy, respectively. For HTD, a significant wall temperature peak is identified ahead of the pseudo-critical point (see Fig. 7c). Normal heat transfer route is assumed from a to b in the wall temperature curve. Wall temperature overshoot ΔT is defined as the wall temperature peak subtracting the wall temperature according to the NHT route. A significant $\Delta T = 90.7$ °C is attained in Fig. 7c.

Effect of SBO on friction pressure drops and friction factors is examined in Fig. 8, including 127 data points for NHT and 97 data points

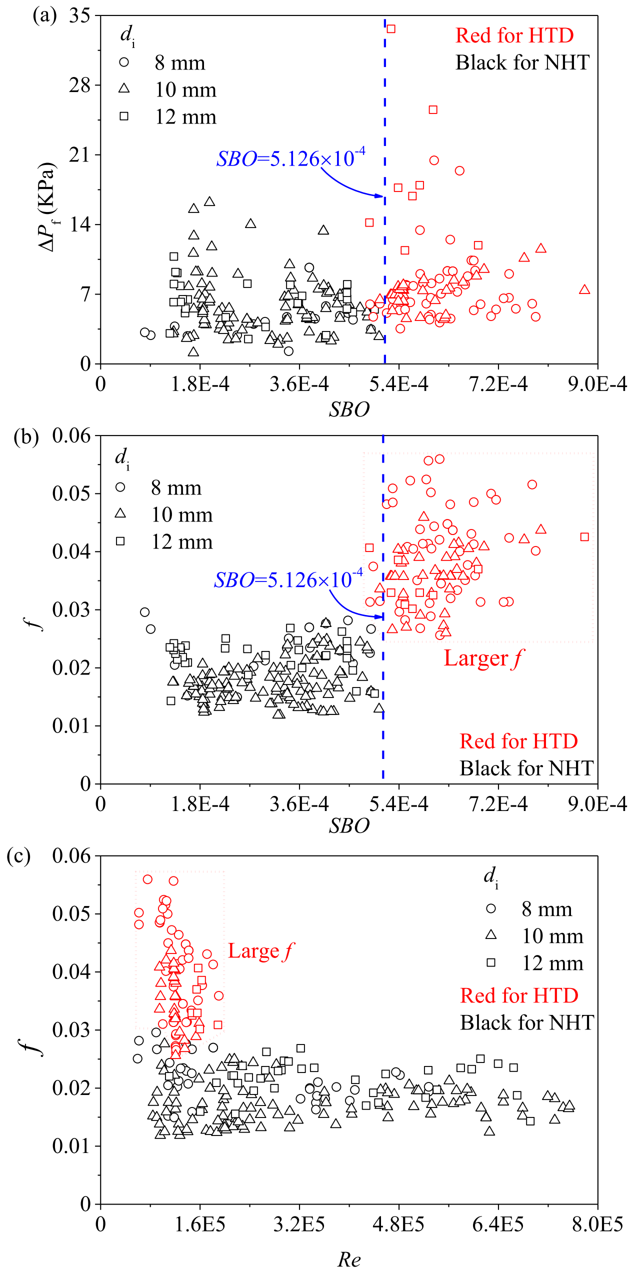

Fig. 8. The two regions of friction pressure drops dependent on *SBO* (ΔP_f versus *SBO*; b: *f* versus *SBO*; c: *f* versus *Re*).

for HTD. Because ΔP_f is dependent on various parameters, both NHT and HTD runs involve similar magnitudes of ΔP_f, except that a couple of data points for HTD have higher ΔP_f up to 34 kPa (see Fig. 8a). As a non-dimensional parameter, *f* is observed to have two regimes distribution, with *f* in the range of 0.01–0.03 for NHT with $SBO < 5.126 \times 10^{-4}$, but in the range of 0.025–0.057 for HTD with $SBO > 5.126 \times 10^{-4}$ (see Fig. 8b). Friction factors *f* are plotted versus *Re* in Fig. 8c, showing that *f* is not only dependent on *Re*, but also dependent on if heat transfer deterioration occurs. With *Re* in the range of 6×10^4–2×10^5, *f* is significantly larger for HTD compared to NHT, displaying the two regimes distribution of friction factors.

4.3. The similarity criterion number and correlation of friction factors

Section 4.2 indicates that *SBO* is an important non-dimensional parameter to characterize both heat transfer and flow resistance. Two findings are summarized as follows: (1) Normal heat transfer is suddenly switched to heat transfer deterioration when crossing a critical $SBO_{cr} = 5.126 \times 10^{-4}$. (2) Friction factors *f* display two regimes distribution, which are smaller for NHT, but are almost doubled for HTD with $SBO > 5.126 \times 10^{-4}$.

SBO can be used to evaluate if a run belongs to NHT or HTD. Meanwhile, *K* defined in Eq. (16) contains inner wall temperature to influence the gas-like GL layer thickness to dominate flow and heat transfer. Effects of *K* on friction pressure drops and wall temperature overshoot are plotted in Fig. 9, noting that each subfigure in Fig. 9 shares similar *P*, *G* and d_i, but different data points have different q_w and *K*. For NHT, *K* is determined at the cross-section having $T_{b,ave}$, but for HTD it is calculated at the cross-section corresponding to wall temperature peak to reflect the orifice contraction effect. Such effect introduces additional pressure drop due to local fluid restriction. It is observed that ΔP_f and ΔT share similar variation trends. In NHT regime represented by black data points, ΔP_f gently increases with increase of *K*, meanwhile ΔT is zero or very small in a couple of degrees. In HTD regime represented by red data points, both ΔP_f and ΔT quickly increase versus *K* and they share the similar trend. The two curves display the similarity characteristic, demonstrating that *K* can be the similarity criterion number to connect flow resistance and heat transfer. A large *K* increases the gas-like GL layer thickness to weaken the heat transfer, thus the wall temperature overshoot is increased. Meanwhile, a larger *K* introduces a larger orifice contraction effect to block the fluid flow, thus pressure drop increases (see Fig. 4c).

Fig. 9 inspires us to present a new friction factor correlation based on *Re* and *K*:

$$f = 2.15Re^{-0.342}K^{0.027} \tag{18}$$

The positive exponent for *K* indicates the increase trend of *f* with increase of *K*. Eq. (18) is suitable for the following data ranges: P = 7.5–23 MPa, G = 500–1500 kg/m^2 s and q_w = 15–400 kW/m^2 with d_i = 8.0, 10.0 and 12.0 mm. Correspondingly, *Re* and *K* cover the ranges of $Re = 5.9 \times 10^4$–7.5×10^5 and $K = 6.4 \times 10^{-8}$–2.7×10^{-6}, respectively. We note that a supercritical pressure corresponds to a pseudo-critical temperature T_{pc}. In order to evaluate the effectiveness of Eq. (18), the non-dimensional temperature $T_{b,ave}/T_{pc}$ is used, where $T_{b,ave}$ is the average fluid temperature between inlet and outlet. Eq. (18) is valid for $T_{b,ave}/T_{pc}$ in the range of 0.8–1.5, indicating that it is correct for the vapor temperature of 50% higher than the pseudo-critical temperature. That is to say, Eq. (18) is valid for fluid temperatures are far away from the pseudo-critical temperature. The effectiveness of Eq. (18) beyond the present data ranges should be verified in the future.

Previously, various correlations have been proposed to predict friction factors of supercritical CO_2 (see Table 2). Fig. 10 compares the present correlation of Eq. (18) with other correlations shown in Table 2, in which f_{pre} is the predicted friction factor using the correlations, and f_{exp} is the experimentally determined ones. The mean relative error (e_A), mean absolute relative error (e_R) and root-mean-square relative error (e_S) characterize the prediction accuracies. For friction factor *f*, the error for a single data point is

$$e_i = \frac{f_{pre} - f_{exp}}{f_{exp}} \tag{19}$$

The three deviation parameters are

$$e_A = \frac{1}{n}\sum_{i=1}^{n} e_i \times 100\%,\ e_R = \frac{1}{n}\sum_{i=1}^{n} |e_i| \times 100\%,\ e_S = \sqrt{\frac{1}{n}\sum_{i=1}^{n} e_i^2} \times 100\% \tag{20}$$

The mean relative error e_A summarizes the overall tendency of the correlation to over-predict or under-predict the measured values. Because e_A concerns the sign of the relative error, positive and negative deviations can offset each other, thus e_A can indicate the error distribution. The mean absolute relative error e_R describes the arithmetic

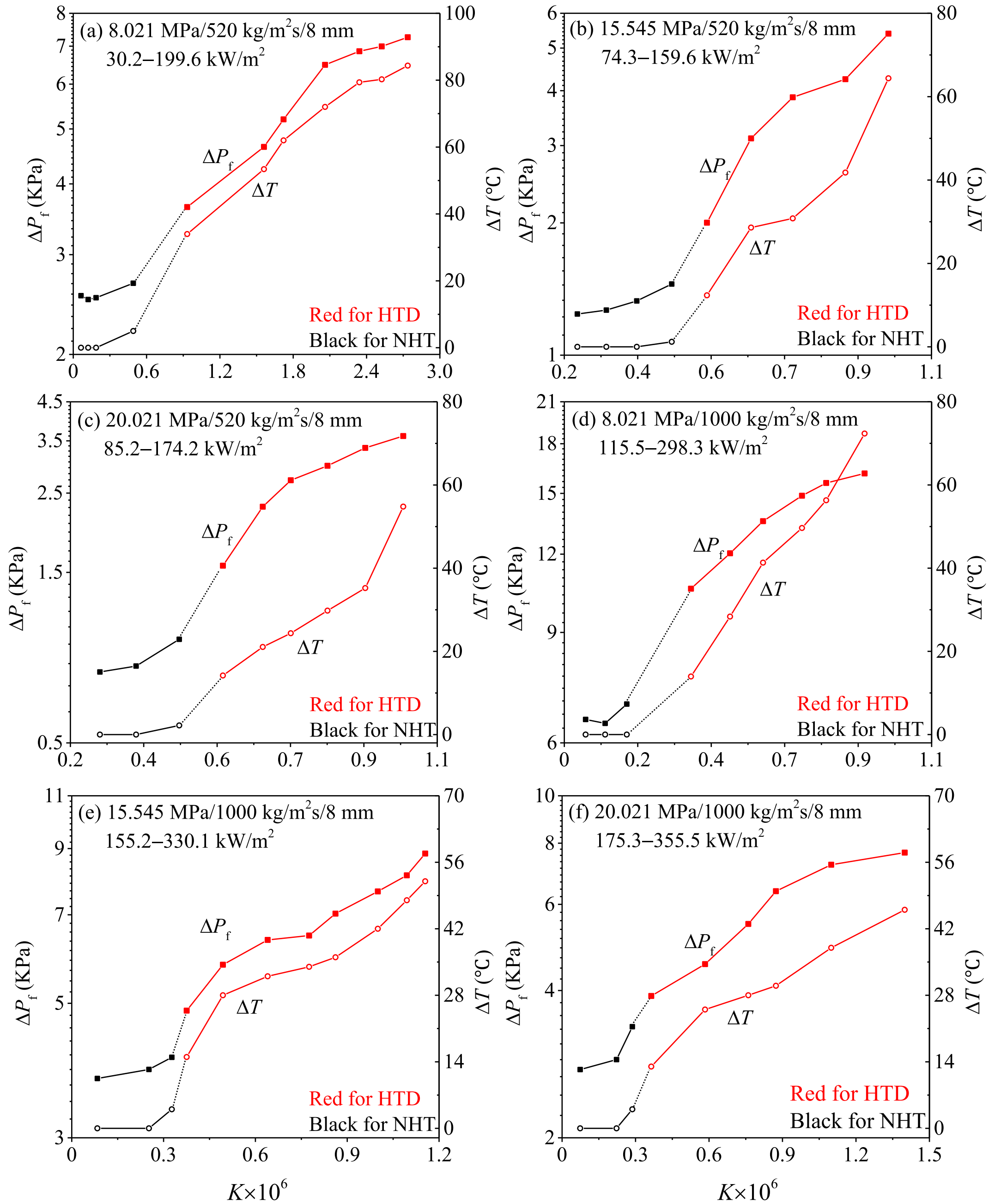

Fig. 9. Effect of K on wall temperature overshoot and friction pressure drops.

Table 2
Available friction factor correlations in references.

References	Correlations	The parameter ranges
Filonenko (1954) [46]	$f = (1.82 log_{10}Re - 1.64)^{-2}$	Single-phase flow, $10^4 \leqslant Re \leqslant 5 \times 10^6$
Popov (1967) [47]	$f = f_{iso}(\rho_{ave}/\rho_b)^{0.74}$, $f_{iso} = (1.82 log_{10}Re - 1.64)^{-2}$, ρ_{ave} is determined by $T_{ave} = (T_w + T_b)/2$	Based on sCO_2 data under cooling condition
Petrov and Popov (1985) [11]	$f = f_{iso,w}\frac{\rho_w}{\rho_b}\left(\frac{\mu_w}{\mu_b}\right)^s$, $f_{iso,w} = (1.82 log_{10}Re_w - 1.64)^{-2}$, $s = 0.023(\lvert q \rvert/G)^{0.42}$	Based on sCO_2 data under cooling condition, $Re_w = 1.4 \times 10^4 - 7.9 \times 10^5$, $Re_b = 3.1 \times 10^4 - 8 \times 10^5$
Wang et al. (2014) [8]	$\frac{1}{\sqrt{f}} = -2.34 lg\left(\frac{\varepsilon_{ab}}{1.72d_i} - \frac{9.26}{Re} \times lg\left(\left(\frac{\varepsilon_{ab}}{29.36d_i}\right)^{0.95} + \left(\frac{18.35}{Re}\right)^{1.108}\right)\right)$	Based on sCO_2 data with $P = 3.5$–40 MPa, $Re = 3400$–2.0×10^6, $T_{in} = 30$–150 °C, $d_i = 1.78$ mm, $\varepsilon_{ab}/d_i = 0.005, 0.015, 0.025$
Fang et al. (2020) [18]	$f = 0.0127\left[ln\left(650\left(\frac{\varepsilon_{ave}}{d_i}\right)^{0.67} + \left(\frac{99000}{Re}\right)^{1.32} + 0.066Ch\right)\right]$, $Ch = \frac{P}{G\sqrt{i - i_0}}$	Based on data of CO_2, R22, R404A, R134a, R410A, RP-3 and H_2O
Present correlation in this paper	$f = 2.15Re^{-0.342}K^{0.027}$	Based on sCO_2 data with $P = 7.5$–23 MPa, $T_{b,ave}/T_{pc} = 0.8$–1.5, $Re = 5.9 \times 10^4$–7.5×10^5 and $K = 6.4 \times 10^{-8}$–2.7×10^{-6}

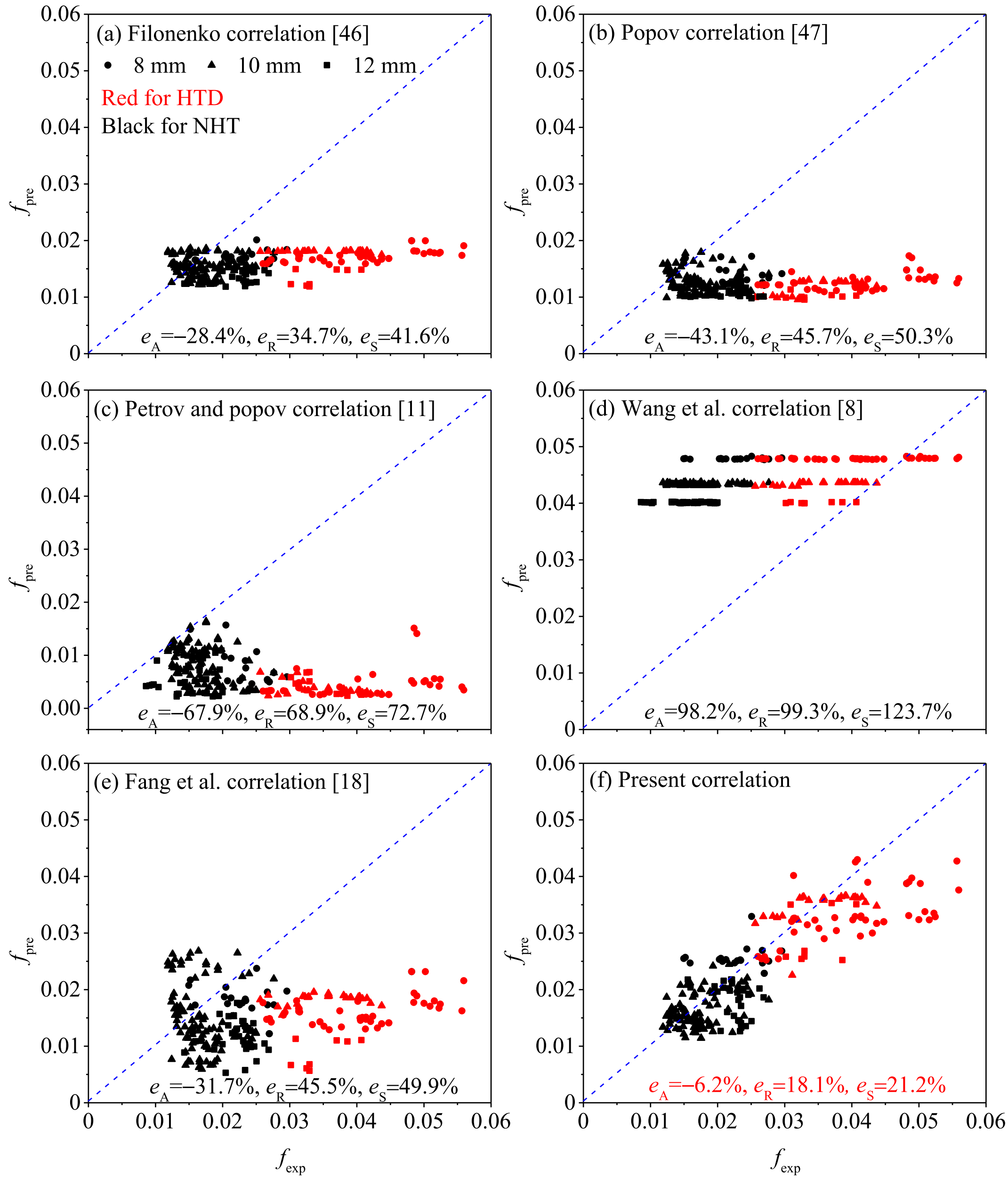

Fig. 10. The comparison between predicted friction factors using various correlations and experiment determined friction factors.

mean of the absolute errors, expressing the correlation accuracy. Alternatively, the root-mean-square relative error e_S emphasizes larger deviations.

Because the Filonenko correlation [46] correlates f as a function of Re only (see Table 2), it is not suitable for supercritical fluids. The three deviation parameters are −28.4%, 34.7% and 41.6%, respectively (see Fig. 10a). The correlations of Popov [47] and Petrov & Popov [11] introduced the correction terms of varied densities and/or viscosities dependent on temperatures. The two correlations significantly under-predict the friction factors by comparing with experiments (see Fig. 10b-c). Wang et al. [8] developed the correlation by introducing tube wall roughness except Re, which significantly over-predicts our experimentally determined friction factors (see Fig. 10d). Fang et al. [18] developed the f correction including a non-dimensional parameter of Ch considering the effect of fluid pressure, mass flux and enthalpy, but the prediction accuracy is not improved (see Fig. 10e). The large deviation between the predicted f using available correlations and our experiments is due to the fact that none of these correlations can predict the flow resistance when heat transfer deterioration occurs. The present correlation of Eq. (18) reasonably agrees with our experiment determined friction factors (see Fig. 10f). The three deviation parameters are $e_A = -6.2\%$, $e_R = 18.1\%$ and $e_S = 21.2\%$, which are the smallest among all the correlations listed in Table 2. It is emphasized that our correlation is not only suitable for normal heat transfer, but also suitable for heat transfer deterioration.

Finally, the error distributions are shown in Fig. 11, containing 127 data points for NHT and 97 data points for HTD. Three tube diameters are involved. We see that the Wang et al. correlation [8] severely over-predict the friction factors, with the maximum error of ~400% (see Fig. 11d). The other three correlations yield the errors in the range of −80% to 80% (see Fig. 11a, b, c and e). Most importantly, the three correlations significantly under-predict f for heat transfer deterioration. On the contrary, the present correlation not only has the capability to predict f for both normal heat transfer and heat transfer deterioration,

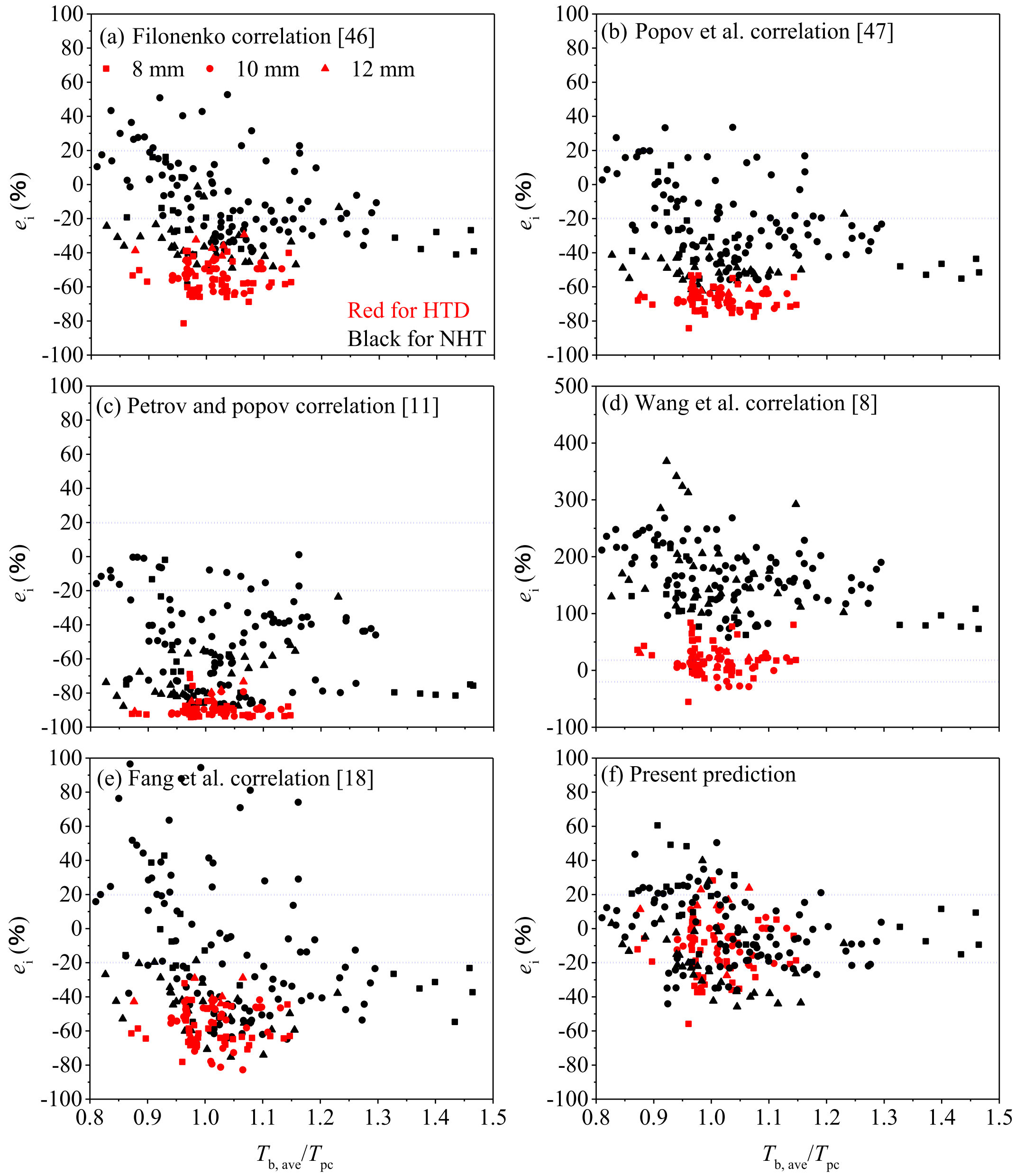

Fig. 11. The error distribution with various correlations in references and present correlation.

but also is suitable when $T_{b,ave}/T_{pc}$ reaches 1.5 (see Fig. 11f).

5. Conclusions

Conclusions are drawn as follows:

- The sCO_2 experiments were performed, with pressures, mass fluxes and heat fluxes in the ranges of 7.5–23 MPa, 500–1500 kg/m^{2}s and 15–400 kW/m^2, respectively. Three inner tube diameters of d_i = 8.0, 10.0 and 12.0 mm are used. New experiment data of pressure drops were reported when heat transfer deterioration occurs.
- Different from classical treatment with single-phase fluid assumption, supercritical fluid is treated by introducing pseudo-boiling, including a gas-like layer on tube wall and a liquid-like fluid in tube core. Supercritical boiling number *SBO* and *K* are found to dominate flow and heat transfer in supercritical domain.
- It is found that when crossing a critical *SBO*, both flow and heat transfer display the two regimes distribution: a normal heat transfer regime with smaller pressure drop and a heat transfer deterioration regime with larger pressure drop.
- The *K* number is identified to be a similarity criterion number, making a connection between pressure drop and heat transfer. Once heat transfer deterioration occurs, the increased pressure drop is explained by the orifice contraction effect due to local vapor expansion to yield vapor plug in tubes, generating additional pressure drop.
- None of the existing correlations in references can predict friction factors during heat transfer deterioration. A new friction factor correlation is developed as a function of *Re* and *K*, which is suitable not only for normal heat transfer, but also for heat transfer deterioration.

Declaration of Competing Interest

The authors declare that they have no known competing financial interests or personal relationships that could have appeared to influence the work reported in this paper.

Acknowledgements

The study was supported by the National Key R&D Program of China (2017YFB0601801), the National Natural Science Foundation of China (51821004) and Fundamental Research Funds for Central Universities (2020DF002).

References

[1] D. Bolmatov, V.V. Brazhkin, K. Trachenko, Thermodynamic behaviour of supercritical matter, Nat. Commun. 4 (2013) 1–7, https://doi.org/10.1016/10.1038/ncomms3331.
[2] J. Xu, E. Sun, M. Li, H. Liu, B. Zhu, Key issues and solution strategies for supercritical carbon dioxide coal fired power plant, Energy 157 (2018) 227–246, https://doi.org/10.1016/j.energy.2018.05.162.
[3] E.H. Sun, J.L. Xu, M.J. Li, G.L. Liu, B.G. Zhu, Connected–top–bottom-cycle to cascade utilize flue gas heat for supercritical carbon dioxide coal fired power plant, Energ. Convers. Manage. 172 (2018) 138–154, https://doi.org/10.1016/j.enconman.2018.07.017.
[4] Y. Ahn, S.J. Bae, M. Kim, S. Cho, Review of supercritical CO_2 power cycle technology and current status of research and development, Nucl. Eng. Technol. 47 (2015) 647–661, https://doi.org/10.1016/j.net.2015.06.009.
[5] X.H. Wang, Q.B. Liu, Z. Bai, J. Lei, H.G. Jin, Thermodynamic investigations of the supercritical CO_2, system with solar energy and biomass, Appl. Energ. 227 (2018) 108–118, https://doi.org/10.1016/j.apenergy.2017.08.00 1.
[6] Y. Yang, W.G. Bai, Y.M. Wang, Y.F. Zhang, H.Z. Li, M.Y. Yao, H.J. Wang, Coupled simulation of the combustion and fluid heating of a 300 MW supercritical CO_2 boiler, Appl. Therm. Eng. 113 (2017) 259–267, https://doi.org/10.1016/j.applthermaleng.2016.11.043.
[7] Y.H. Fan, G.H. Tang, Numerical investigation on heat transfer of supercritical carbon dioxide in a vertical tube under circumferentially non-uniform heating, Appl. Therm. Eng. 138 (2018) 354–364, https://doi.org/10.1016/j.applthermaleng.2018.04.060.
[8] Z.Y. Wang, B.J. Sun, J.T. Wang, L. Hou, Experimental study on the friction coefficient of supercritical carbon dioxide in pipes, Int. J. Greenh. Gas Con. 25 (2014) 151–161, https://doi.org/10.1016/j.ijggc.2014.04.014.
[9] I.L. Pioro, R.B. Duffey, T.J. Dumouchel, Hydraulic resistance of fluids flowing in channels at supercritical pressures (survey), Nucl. Eng. Des. 231 (2) (2004) 187–197, https://doi.org/10.1016/j.nucengdes.2004.03.001.
[10] C.R. Zhao, P.X. Jiang, Experimental study of in-tube cooling heat transfer and pressure drop characteristics of R134a at supercritical pressures, Exp. Therm. Fluid Sci. 35 (2011) 1293–1303, https://doi.org/10.1016/j.expthermflusci.2011.04.017.
[11] N.E. Petrov, V.N. Popov, Heat-transfer and resistance of carbon-dioxide being cooled in the supercritical region, Therm. Eng. 32 (1985) 131–134. https://www.researchgate.net/publication/287004265.
[12] P.X. Jiang, C.R. Zhao, B. Liu, Flow and heat transfer characteristics of r22 and ethanol at supercritical pressures, J. Supercrit. Fluids 70 (2012) 75–89, https://doi.org/j.supflu.2012.06.011.
[13] X.D. Fang, Y. Xu, X.H. Su, R.R. Shi, Pressure drop and friction factor correlations of supercritical flow, Nucl. Eng. Des. 242 (2012) 323–330, https://doi.org/j.nucengdes.2011.10.041.
[14] C. Zhang, G. Xu, H. Deng, K. Zhu, Investigation of flow resistance characteristics of endothermic hydrocarbon fuel under supercritical pressures, Propulsion and Power Research 2 (2) (2013) 119–130, https://doi.org/j.jppr.2013.04.002.
[15] S. Garimella, B. Mitra, U.C. Andresen, Y. Jiang, B.M. Fronk, Heat transfer and pressure drop during supercritical cooling of HFC refrigerant blends, Int. J. Heat Mass Tran. 91 (2015) 477–493, https://doi.org/j.ijheatmasstransfer.2015.07.024.
[16] H. Wang, Q.C. Bi, G. Wu, Z.D. Yang, Experimental investigation on pressure drop of supercritical water in an annular channel, J. Supercrit. Fluids 131 (2018) 47–57, https://doi.org/j.supflu.2017.08.014.
[17] J.G. Zang, X. Yan, Y.L. Li, X.K. Zeng, Y.P. Huang, The flow resistance experiments of supercritical pressure water in 2×2 rod bundle, Int. J. Heat Mass Tran. 147 (2020) 118873, https://doi.org/j.ijheatmasstransfer.2019.118873.
[18] X. Fang, L.u. Xu, Y. Chen, W. Chen, Correlations for friction factor of turbulent pipe flow under supercritical pressure: Review and a new correlation, Prog. Nucl. Energy 118 (2020), https://doi.org/10.1016/j.pnucene.2019.103085.
[19] R.B. Duffey, I.L. Pioro, Heat transfer and hydraulic resistance at supercritical pressures in power engineering applications, ASME Press Am. (2007) 175–210, https://doi.org/10.1115/1.802574.bm.
[20] M.M. Ehsan, Z. Guan, A.Y. Klimenko, A comprehensive review on heat transfer and pressure drop characteristics and correlations with supercritical CO_2 under heating and cooling applications, Renew. Sust. Energ. Rev. 92 (2018) 658–675, https://doi.org/j.rser.2018.04.106.
[21] D. Huang, W. Li, A brief review on the buoyancy criteria for supercritical fluids, Appl. Therm. Eng. 131 (2018) 977–987, https://doi.org/10.1016/j.applthermaleng.2017.12.042.
[22] P.L. Kirillov, Y.S. Yurev, V.P. Bobkov, Handbook of Thermal-Hydraulic Calculations, Energoatomizdat Publishing House, Moscow, 1990.
[23] B.S. Petukhov, V.A. Kurganov, V.B. Ankudinow, Heat transfer and flow resistance in the turbulent pipe flow of a fluid with near-critical state parameters, High Temp. 21 (1983) 81–89, https://doi.org/0011-2275(83)90066–8.
[24] M.A. Mikheev, Fundamentals of Heat Transfer, Gosenergoizdat Publishing House, Moscow, 1956.
[25] M. Pizzarelli, The status of the research on the heat transfer deterioration in supercritical fluids: a review, Int. Commun. Heat Mass Transf. 95 (2018) 132–138, https://doi.org/10.1016/j.icheatmasstransfer.2018.04.006.
[26] H.F. Gu, H.Z. Li, H.J. Wang, Y.S. Luo, Experimental investigation on convective heat transfer from a horizontal miniature tube to methane at supercritical pressures, Appl. Therm. Eng. 58 (2013) 490–498, https://doi.org/10.1016/j.applthermaleng.2013.04.049.
[27] I. Pioro, Application of Supercritical Pressure in Power Engineering, in: Supercritical Fluid Technology for Energy and Environmental Applications, Elsevier B.V., Netherlands, 2014, pp. 201–233, https://doi.org/10.1016/B978–0–444–62696–7.00011–3.
[28] Q. Zhang, H.X. Li, X.F. Kong, J.L. Liu, X.L. Lei, Special heat transfer characteristics of supercritical CO_2 flowing in a vertically-upward tube with low mass flux, Int. J. Heat Mass Tran. 122 (2018) 469–482, https://doi.org/j.ijheatmasstransfer.2018.01.112.
[29] E.H. Sun, H. Hu, H.N. Li, J.L. Xu, G.H. Liu, Concept design of Supercritical CO_2 cycle driven by pressurized fluidized bed combustion (PFBC) boiler, Appl. Therm. Eng. 166 (2020), 114756, https://doi.org/10.1016/j.applthermaleng.2019.114756.
[30] Z.B. Liu, Y.L. He, Y.F. Yang, J.Y. Fei, Experimental study on heat transfer and pressure drop of supercritical CO_2 cooled in a large tube, Appl. Therm. Eng. 70 (2014) 307–315, https://doi.org/10.1016/j. applthermaleng.2014.05.024.
[31] H. Wang, K.H. Leung, W.S. Wang, Q.C. Bi, A review on recent heat transfer studies to supercritical pressure water in channels, Appl. Therm. Eng. 142 (2018) 573–596, https://doi.org/10.1016/j.applthermaleng. 2018.07.007.
[32] J.Z. Xie, D.C. Liu, H.B. Yan, G.N. Xie, S.K.S. Boetcher, A review of heat transfer deterioration of supercritical carbon dioxide flowing in vertical tubes: Heat transfer behaviors, identification methods, critical heat fluxes, and heat transfer correlations, Int. J. Heat Mass Tran. 149 (2020) 119233, https://doi.org/10.1016/j.ijheatmasstransfer.2019.119233.
[33] G.G. Simeoni, T. Bryk, F.A. Gorelli, M. Krisch, G. Ruocco, M. Santoro, T. Scopigno, The Widom line as the crossover between liquid-like and gas-like behavior in supercritical fluids, Nat. Phys. 6 (2010) 503–507, https://doi.org/10.1038/nphys1683.
[34] P.F. McMillan, H.E. Stanley, Going supercritical, Nature Phys. 6 (7) (2010) 479–480, https://www.nature.com/naturephysics.
[35] M.Y. Ha, T.J. Yoon, T. Tlusty, Y. Jho, W.B. Lee, Widom delta of supercritical gas–liquid coexistence, J. Phys. Chem. Lett. 9 (7) (2018) 1734–1738, https://doi.org/10.1021/acs.jpclett.8b00430.
[36] F.A. Gorelli, T. Bryk, M. Krisch, G. Ruocco, M. Santoro, T. Scopigno, Dynamics and thermodynamics beyond the critical point, Sci. Rep. 3 (2013), https://doi.org/10.1038/srep01203.
[37] J.W. Ackerman, Pseudoboiling heat transfer to supercritical pressure water in smooth and ribbed tubes, J. Heat Transf. 92 (3) (1970) 490–497, https://doi.org/10.1115/1.3449698.
[38] K. Nishikawa, K. Miyabe, On the Boiling-Like phenomena at supercritical pressures, Mem. Fac. Eng., Kyushu Univ. 25 (1965) 1–25, https://www.osti.gov/biblio/4457213.
[39] B. Widom, Surface tension and molecular correlations near the critical point, J. Chem. Phys. 43 (11) (1965) 3892–3897.
[40] F. Maxim, C. Contescu, P. Boillat, B. Niceno, K. Karalis, A. Testino, C. Ludwig, Visualization of supercritical water pseudo–boiling at Widom line crossover, Nat. Commun. 10 (2019) 1–11, https://doi.org/10.1038/s41467-019-12117-5.
[41] S.G. Kandlikar, Heat transfer mechanisms during flow boiling in microchannels, J. Heat Transf. 126 (2004) 8–16, https://doi.org/10.1115/1.1643090.
[42] B. Zhu, J. Xu, X. Wu, J. Xie, M. Li, Supercritical "boiling" number, a new parameter to distinguish two regimes of carbon dioxide heat transfer in tubes, Int. J. Therm. Sci. 136 (2019) 254–266, https://doi.org/j.ijthermalsci.2018.10.032.
[43] J. Xu, H. Zhang, B. Zhu, J. Xie, Critical supercritical-boiling-number to determine the onset of heat transfer deterioration for supercritical fluids, Sol. Energy 195 (2020) 27–36, https://doi.org/j.solener.2019.11.036.
[44] B.G. Zhu, J.L. Xu, C.S. Yan, J. Xie, The general supercritical heat transfer correlation for vertical up-flow tubes: K number correlation, Int. J. Heat Mass Tran. 148 (2020) 119080, https://doi.org/j.ijheatmasstransfer.2019.119080.
[45] A.V. Solov'ev, E.I. Preobrazhenskii, P.A. Semenov, Hydraulic resistance in two-phase flow, Int. Chem. Eng. 7 (1967) 59–63, https://www.researchgate.net/publication/282405607.
[46] G.K. Filonenko, Hydraulic resistance of pipelines, Therm. Eng. 4 (1954) 40–44.
[47] V.N. Popov, Theoretical calculation of heat transfer and friction resistance for supercritical carbon dioxide. In: J.P. Hartnett, E.R.C. Ecker, (Eds.), Proceedings of Second All–Soviet Union Conference on Heat and Mass Transfer, Minsk, 1964, pp. 46–56.